

Tailorable optical scattering properties of V-shaped plasmonic nanoantennas: a computationally efficient and fast analysis

Arash Rashidi,¹ M. T. Chryssomallis,² and D. E. Anagnostou^{2,3,*}

¹*EcoMotors, 17000 Federal Drive, Allen Park, Michigan 48101, USA*

²*Electrical and Computer Engineering Department, Democritus University of Thrace, Xanthi 67100, Greece*

³*Electrical and Computer Engineering Department, South Dakota School of Mines & Technology, Rapid City, South Dakota 57701, USA*

*Corresponding author: danagn@ieee.org

Received June 11, 2014; revised July 30, 2014; accepted August 25, 2014;
posted August 26, 2014 (Doc. ID 213914); published September 19, 2014

In this work, we introduce an efficient computational scheme, based on the macro basis function method, to analyze the scattering of a plane wave by V-shaped plasmonic optical nanoantennas. The polarization currents and scattered fields for the both symmetric and antisymmetric excitations are investigated. We investigate how the resonant frequency of the plasmonic V-shaped nanoantenna is tailored by engineering the geometrical parameters and by changing the polarization state of the incident plane wave. The computational model presented herein is faster by many orders of magnitude than commercially available finite methods, and is capable of characterizing all nanoantennas comprised of junctions and bends of nanorods. © 2014 Optical Society of America

OCIS codes: (160.3918) Metamaterials; (250.5403) Plasmonics; (290.0290) Scattering.

<http://dx.doi.org/10.1364/JOSAA.31.002256>

1. INTRODUCTION

Plasmonic nanoantennas have recently been used in photovoltaic devices, biosensing, nonlinear optics, quantum optics, and optical circuits [1,2]. Wire plasmonic nanoantennas recently have been studied and characterized, which allow only one scattered electric field component along the nanorod axis [3,4]. However, controlling the polarization state of photons is required in some optical applications, e.g., cryptography, optical computing, and communications [5]. Cross-resonant plasmonic nanoantennas consisting of two perpendicular plasmonic dipole antennas have been shown that are capable of converting propagating fields of any polarization state into correspondingly polarized, localized, and enhanced fields and vice versa [6,7]. Other plasmonic nanoantennas comprised of junctions that connect six or eight monopoles have been introduced to obtain a broadband spectral response when illuminated with circular and elliptical polarizations [8].

The basic idea to make plasmonic wire nanoantennas capable of illustrating versatile polarization states for photons is realized by having a set of noncollinear monopoles. In this configuration, each monopole radiates an electric field polarized in parallel to the corresponding axis. Because the monopoles are not collinear, different polarization states for the total scattered field are achieved. The simplest way to get a noncollinear set of coupled monopoles is by introducing a V-shaped plasmonic nanoantenna consisting of two arms of equal length $L/2$ connected at one end at an angle Δ , as illustrated in Fig. 1.

There recently has been significant interest in V-shaped plasmonic nanoantennas because of their special phase response when spatially tailoring their geometry, i.e., L and

Δ , in an array [9]. Such arrays of plasmonic V-antennas have been shown that are capable of molding the wavefront of the reflected and refracted beams in a nearly arbitrary way. The other advantages of V-shaped plasmonic nanoantennas are the ease of fabricating planar antennas of nanoscale thickness and the fact that such V-shaped antennas consist of plasmonic nanorod resonators having widely tailorable optical properties [10,11]. The main question is how we can analyze efficiently and quickly the optical performance of the V-shaped plasmonic antenna to investigate its importance as a fundamental nanoelement in plasmonic optics in changing the polarization state and phase of photons, while giving rise to the geometrically tunable resonances to get a strong enough magnitude of the scattered field.

To facilitate the design of optical metamaterials comprising V-shaped nanoantennas, an efficient formulation is needed to quantify their optical performance. Conventional electromagnetic-simulation (EM) packages, which usually use a finite difference time-domain (FDTD) technique, are often either inaccurate or highly time- and memory-consuming. This is mainly because FDTD requires a fine meshing to characterize the thin cross-sections of the nanorod comprised of dispersive and negative-permittivity material [12,13].

The macro basis function (MBF) method has been found to be a time- and memory-efficient technique for analyzing the scattering from the plasmonic nanorod antennas [13], and also for the scattering analysis of elements comprising junctions of wires and strips in the microwave regime [14]. The main advantages of utilizing the MBF method are (1) they demonstrate a relatively small-sized and well-conditioned matrix equation; (2) they are faster in speed and require less memory, by 4 to 10 orders of magnitude, than the conventional numerical

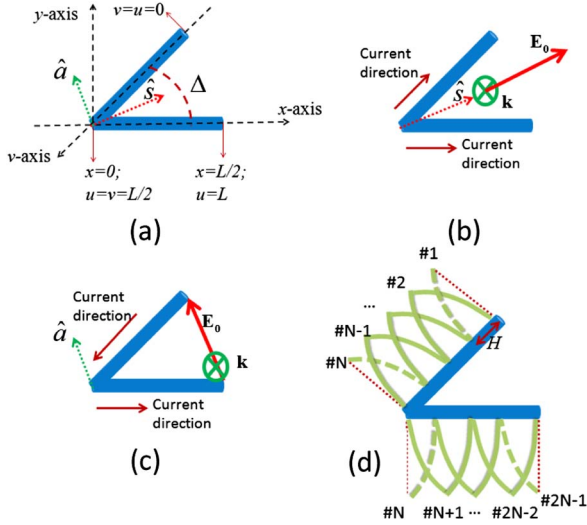


Fig. 1. (a) Geometry of V-shaped plasmonic nanoantennas. (b) Symmetric mode. (c) Antisymmetric mode. (d) Discretization of the polarization current.

methods; (3) they propose a computationally efficient scheme to model the current at the junction of elements, e.g., cross-shaped elements, by satisfying Kirchhoff current law (KCL) and obviating the need to handle fictitious singularities of the electric field generated by piecewise sinusoidal Basis Functions at the junction [14]; (4) they demonstrate the closed-form formula for the radiated electric field generated by MBFs [13]; and (5) they are compatible with the characteristic basis function method to efficiently characterize the scattering performance of infinite and large finite clusters of metamaterials [15]. In this work, we use the MBF method to analyze the scattering performance of the V-shaped plasmonic nanoantenna to take advantage of all the above-mentioned improving features.

2. SCATTERING FROM A PLASMONIC V-SHAPED NANOANTENNA

This section demonstrates the formulation for the problem at hand. Figure 1(a) demonstrates a V-shaped plasmonic nanoantenna located in the xy plane, which consists of two arms of equal length $L/2 = 75$ nm and equal radius $a = 7.5$ nm connected at one end at an angle Δ . One arm is along the x axis and the other arm is along the v axis. We parameterize the combination of the v - and x -axes with the u parameter such that $0 \leq u \leq L$ [see Fig. 1(a)]. Both arms are made of silver, by which its permittivity is characterized by Drude model, i.e., $\epsilon_r = \epsilon_{r\infty} - f_p^2 / [f(f - jf_d)]$, with $\epsilon_{r\infty} = 5$, $f_p = 2175$ THz and $f_d = 4.35$ THz, where f_p is the plasma frequency and f_d is the damping frequency [13]. We define two unit vectors to describe the orientation of a V-antenna: \hat{s} , along the symmetry axis of the antenna (the bisector of the angle Δ) and \hat{a} , perpendicular to \hat{s} [see Fig. 1(a)]. V-antennas support “symmetric” and “antisymmetric” modes [see Figs. 1(b) and 1(c)] [9]. Physically, for a single plasmonic nanorod antenna illuminated by an arbitrarily incident plane wave [13], the longitudinal polarization current is excited by the vector component of the incident electric field, which is directed along the axis of the nanorod (let us neglect the effect of the transverse polarization current in the cross-section of

the nanorod because of the thin cross-section). Keeping this in mind, for the symmetric excitation, when the incident electric field is along \hat{s} [see Fig. 1(b)], the polarization current in each arm is directed from the junction end toward the open end of the corresponding arm. Similarly for the antisymmetric excitation, when the incident electric field is along \hat{a} as depicted in Fig. 1(c), by projecting the incident electric field onto each arm, the direction of the currents is along \hat{x} (for the x arm) and \hat{v} (for the v arm), respectively. The incident wave vector \mathbf{k} for both symmetric and antisymmetric modes is inward and normal to the plane of the device, i.e., $-\hat{z}$ [see Figs. 1(b) and 1(c)].

One way to solve the scattering performance of a dielectric body of relative permittivity ϵ_r , illuminated by the incident electric field \mathbf{E}^{Inc} , is using the volume-equivalent theorem [16]. In this theorem, we replace the dielectric material with a polarization current density \mathbf{J} . The electric field radiated by such a polarization current density is then equivalent to the field \mathbf{E}^{Scat} scattered by the original dielectric body. The polarization current density is proportional to the total electric field \mathbf{E}^{Tot} , the summation of the incident and scattered electric field, as

$$\mathbf{J} = j\omega\epsilon_0(\epsilon_r - 1)\mathbf{E}^{\text{Tot}}, \quad (1)$$

where $e^{j\omega t}$ time dependency for the electric field and polarization current is assumed and suppressed. The first author has applied the volume-equivalent theorem to efficiently characterize the optical scattering performance of plasmonic nanorods in [13]. We use the same theorem in this work for scattering analysis of the V-shaped plasmonic nanoantennas.

By using Eq. (1), the equivalent polarization current on the V-antenna, flowing along the v - and x -directions for the v - and x -arms, respectively, satisfies the following set of polarization equations [13]:

$$\begin{cases} E_{vv}^{\text{scat}} + E_{vx}^{\text{scat}} + E_v^{\text{inc}} = \zeta I_v(v) & \text{on } v\text{-arm} \\ E_{xv}^{\text{scat}} + E_{xx}^{\text{scat}} + E_x^{\text{inc}} = \zeta I_x(x) & \text{on } x\text{-arm} \end{cases}, \quad (2)$$

where E_{wt}^{Scat} is the w -component of the electric field scattered by the t -arm, $t, w \in \{v, x\}$, which is measured along a line segment on the top of the surface of the t -arm parallel to its axis. Because the normal to the plane of the V-antenna is the z axis (see Fig. 1), the location of the observation line segment is at $z = a$, i.e., the distance between the observation line segment on the t -arm and the axis of the t -arm is equal to the radius of the nanorod. E_t^{inc} is the t -component of the incident electric field on the t -arm. The $I_t(t)$ in Eq. (2) is the polarization current flowing on the axis of the t -arm, which is an unknown function yet to be determined. And finally, $\zeta = -j\eta / [\pi a^2 k(\epsilon_r - 1)]$, where η and k are the intrinsic impedance and wave number of the free space, respectively.

To solve Eq. (2) with the MBF method according to the recipe discussed in [13], we expand the polarization current in terms of $2N - 1$ piecewise sinusoidal MBFs [see Fig. 1(d)]. The first and the last MBFs, #1 and $2N - 1$, are half MBFs with the domain width of H to model the nonzero current at the two ends of the V-antenna. The other MBFs are full triangular sinusoidal basis functions with the domain width of $2H$. The MBF# N at the junction is the composite MBF comprised of a half-MBF on the v -arm and another half-MBF on the x -arm

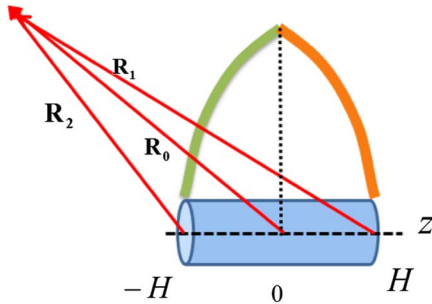


Fig. 2. Full-triangular sinusoidal MBF including right and left MBFs. The current flows along the axis.

with equal current at the junction, i.e., $I_v(v = L/2) = I_x(x = 0)$, which automatically satisfies the KCL.

The details about the current distribution and the radiated electric field associated with piecewise sinusoidal MBFs have been discussed in [13]. However, for the sake of simplicity, we only bring the resultant formulas into our work. Let us consider a full triangular-sinusoidal MBF, including left and right half MBFs as shown in Fig. 2. In this example, the axis of the nanorod is along the z axis; therefore, for the problem at hand (V-shaped nanoantenna in Fig. 1), the proper coordinate rotations must be carried out to use the electric field expressions which we present for the MBFs in Fig. 2. The current is assumed to exist only at the axis of the rod along the z -direction. The current is assumed to have a triangular-sinusoidal variation given by $I_z = \sin[\beta(H - |z'|)]$, where $-H < z' < H$. The z -component of the electric field radiated by the right-half MBF, $0 < z' < H$, is given by

$$G_{zz} = \frac{-j\eta}{4\pi} \left[\frac{e^{-jkR_1}}{R_1} - \frac{e^{-jkR_0}}{R_0} \right] \left(\cos(kH) + j \frac{z}{R_0} \sin(kH) \right) - z \sin(kH) \frac{e^{-jkR_0}}{kR_0^3}, \quad (3)$$

where R_0 and R_1 are the distances from the observation point to the middle ($z' = 0$) and the right end ($z' = H$) of the MBF depicted in Fig. 2. Similarly, as derived in [13], the x -component of the electric field radiated by the right-half MBF depicted in Fig. 2 is

$$G_{xz} = \frac{j\eta x}{4\pi\rho^2} \left\{ z \left[\frac{e^{-jkR_1}}{R_1} - \frac{e^{-jkR_0}}{R_0} \right] \left(\cos(kH) + j \frac{z}{R_0} \sin(kH) \right) + \sin(kH)\rho^2 \frac{e^{-jkR_0}}{kR_0^3} - H \frac{e^{-jkR_1}}{R_1} \right\}. \quad (4)$$

For the y -component of the radiated electric field by the right-half MBF depicted in Fig. 2, it is sufficient to replace the observation component y by x . The electric field radiated by the left-half MBF depicted in Fig. 2 (for which $-H < z' < 0$) is obtained from Eqs. (3),(4) when H is replaced by $-H$.

After expanding the arm currents $I_v(v)$ and $I_x(x)$ in terms of MBFs defined in Fig. 1, we expand the electric fields radiated by the arm currents E_{tot}^{Scat} , where $t, w \in \{v, x\}$ in terms of the electric field radiated by each MBF, using the closed form formulas presented in Eqs. (3),(4) and the corresponding rotation of coordinate system. We therefore have $2N - 1$ unknowns associated with the $2N - 1$ weighting coefficients of MBFs. If we multiply both sides of Eq. (2) by each of the MBFs defined in

Fig. 1, and take the integration along the MBF domain (Galerkin's testing) [13], we achieve a $(2N - 1) \times (2N - 1)$ matrix equation. The integration in the Galerkin's testing is carried out using the Gaussian quadrature rule (GQR) [13]. For each arm, 20 observation points in GQR render the scheme convergent. Solving the resultant matrix equation leads to finding the polarization current and, therefore, we compute the scattered field by the nanoantenna. We need to mention that the size of the matrix equation to reach to a convergent result is relatively small, e.g., only a 5×5 matrix equation (for $100 \text{ THz} \leq f \leq 400 \text{ THz}$) or a 7×7 matrix equation (for $400 \text{ THz} < f \leq 600 \text{ THz}$) can efficiently and accurately model the scattering from the V-shaped plasmonic nanoantenna.

3. SYMMETRIC AND ANTISYMMETRIC EXCITATIONS

For the symmetric and antisymmetric excitations at $f = 200 \text{ THz}$ and for different values of angle Δ , the magnitude and phase of the polarization currents are plotted versus u/L in Figs. 3 and 4. In Fig. 3(a), the current is zero at the junction for the symmetric excitation. This happens because the KCL is set at the junction and is also due to the symmetric excitation [see Fig. 1(b)]. Only a zero current can be present at the junction because of these two constraints. The other observation in Fig. 3(a) is that for $\Delta = 180^\circ$, in which the two arms are collinear and the V-antenna degenerates to a nanorod, there is no polarization current generated by the symmetric excitation. This is because, in this case, the incident electric field is perpendicular to the axis of the nanorod and is not coupled to any longitudinal plasmonic mode in the nanorod.

In Fig. 3(b), for the symmetric excitation, the phase of the polarization current jumps as much as 180° at the junction, which is consistent with the physics, i.e., KCL and symmetric excitation, described previously. On the other hand, the magnitude of the current for the antisymmetric case, in Fig. 4(a), has a peak value at the junction, and the phase at the junction is continuous and almost flat over the V-antenna for $0 \leq u \leq L$. The condition number for the 5×5 impedance matrix is only 35.8 at $f = 200 \text{ THz}$ for $\Delta = 30^\circ$, which is a well-conditioned

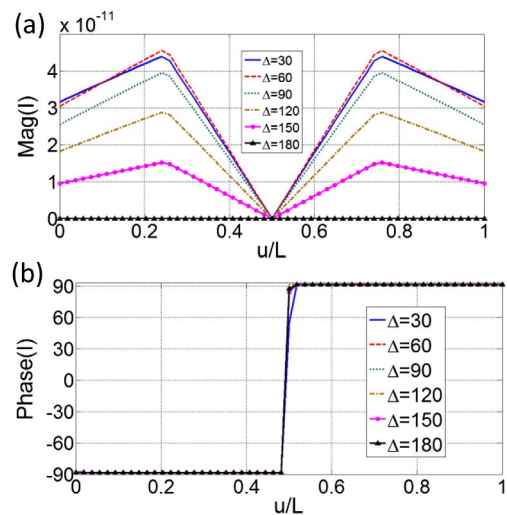


Fig. 3. Polarization current of the V-shaped plasmonic antenna illuminated by a symmetric excitation at $f = 200 \text{ THz}$ ($\lambda = 1.5 \mu\text{m}$) for different values of the angle Δ . (a) Magnitude, (b) phase.

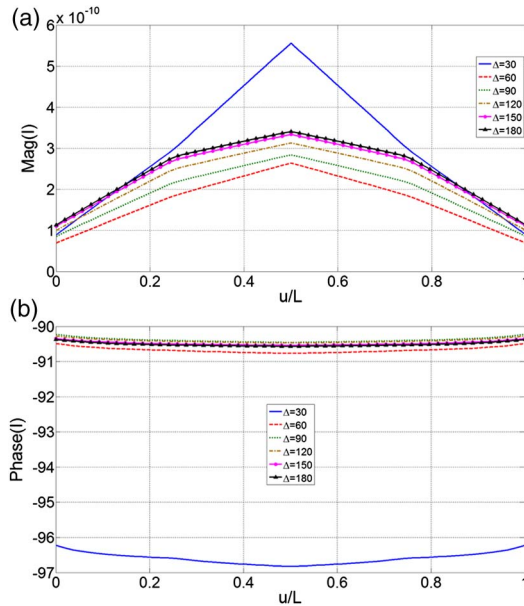


Fig. 4. Polarization current of the V-shaped plasmonic antenna illuminated by an antisymmetric excitation at $f = 200$ THz ($\lambda = 1.5 \mu\text{m}$) for different values of the angle Δ . (a) Magnitude, (b) phase.

matrix. The condition number is even better for greater angles; e.g., for $\Delta = 180^\circ$, the condition number is only 6.8.

The scattered field by the plasmonic V-antenna is the electric field radiated by the determined polarization current. Traditionally the electric field radiated by the given current can be found by performing the convolution of the free space Dyadic Green's function (DGF) and the current. Our computational model obviates the need of using DGFs, because the polarization current in the V-antenna is a superposition of piecewise sinusoidal MBFs and the electric field radiated by each MBF is obtained in a closed-form formula, as described before via Eqs. (3),(4).

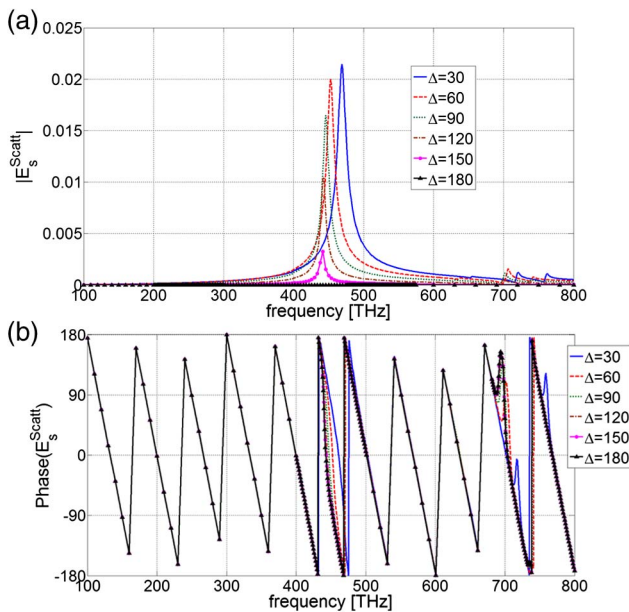


Fig. 5. Scattered field from the V-shaped plasmonic antenna illuminated by a symmetric excitation for different values of the angle Δ . (a) Magnitude, (b) phase.

Figures 5 and 6 illustrate the magnitude and phase of the scattered field by the plasmonic V-shaped nanoantenna observed at $\mathbf{r} = 4.5 [\mu\text{m}]\hat{\mathbf{z}}$ (3λ at 200 THz) for symmetric and antisymmetric modes, respectively. It is interesting to note that for the plasmonic V-antenna, the polarization state of the scattered photons is the same as that of the incident light when the latter is polarized along $\hat{\mathbf{a}}$ or $\hat{\mathbf{s}}$. This means the scattered field is symmetric when the V-antenna is illuminated by a symmetric excitation and is antisymmetric when illuminated by an antisymmetric incident field. This property of the plasmonic V-antenna allows one to design the polarization of the scattered light [9].

In Fig. 5(a), for the symmetric mode, the first-order resonant frequency for which the magnitude of the scattered field is maximum occurs when the length of each arm is around one half of the effective wavelength, i.e., $L/2 = \lambda_{\text{eff}}/2$, because according to Fig. 3, the current distribution in each arm approximates that of an individual straight antenna of length $L/2$ [9].

According to the approximated algebraic formula for the effective wavelength for a plasmonic nanorod given by Novotny [17], the first-order resonant frequency for the symmetric mode for the silver V-antenna studied herein is around $f_{\text{res}} = 415$ THz. According to our computation depicted in Fig. 5(a), f_{res} varies from 469 THz (for $\Delta = 30^\circ$) to 441 THz (for $\Delta = 150^\circ$). The main reason that the resonant frequency of the V-shaped nanoantenna is different from Novotny's result is because in Novotny's formula only one single (isolated) arm is considered, while here we have two arms. Also, there is an electromagnetic coupling between the arms' polarization currents that makes the resonant frequency to deviate from that given by Novotny for an isolated arm. It is interesting to note that the deviation in the resonant frequency is increased for the case $\Delta = 30^\circ$ (in which the arms are closer and more coupled) compared to $\Delta = 150^\circ$, where there is less coupling between the arms.

In Fig. 4(b), we observe that the phase of the scattered field across the resonance changes appreciably, which makes the

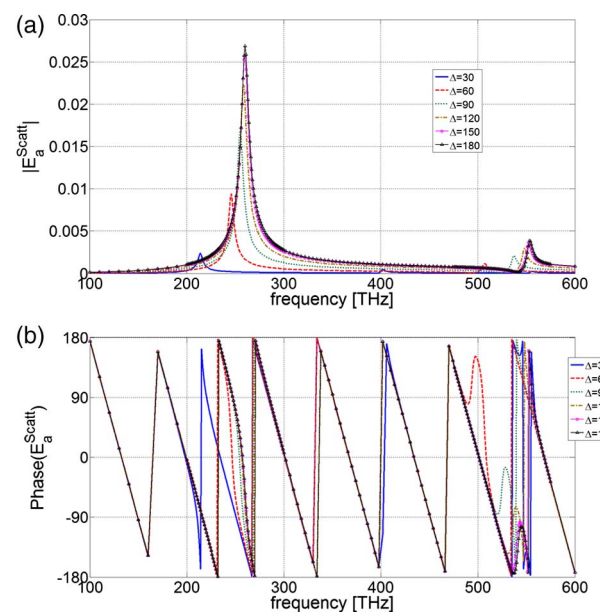


Fig. 6. Scattered field from the V-shaped plasmonic antenna illuminated by an antisymmetric excitation for different values of the angle Δ . (a) Magnitude, (b) phase.

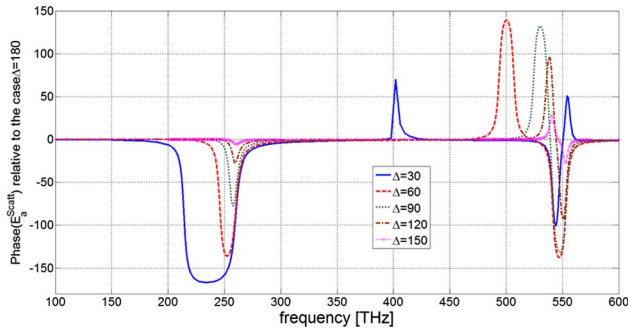


Fig. 7. Phase of the scattered field for the antisymmetric case shifted from the reference phase of the scattered field for $\Delta = 180^\circ$.

plasmonic V-shaped antenna capable of being utilized as an optical resonator to design the magnitude, phase, and polarization state of the scattered light [9]. Similarly, for the antisymmetric excitation, one can conclude that the first-order resonance occurs when $L = \lambda_{\text{eff}}/2$, which is roughly $f_{\text{res}} = 292$ THz. More accurately, according to Fig. 6(a), for the antisymmetric excitation, f_{res} varies from 214 THz (for $\Delta = 30^\circ$) to 260 THz (for $\Delta = 180^\circ$). To facilitate the observation of appreciable phase variation of the scattered field around the resonance, in Fig. 7, for the antisymmetric case, the phase of the scattered field shifted from that of the scattered field for $\Delta = 180^\circ$, i.e., $\angle E_a^{\text{Scatt}}(\Delta) - \angle E_a^{\text{Scatt}}(\Delta = 180^\circ)$ is plotted versus the frequency for different Δ angles.

As the frequency increases, the V-antenna gets higher resonant modes. According to Figs. 5(a) and 6(a), the first resonant frequency of the antisymmetric case is lower than the symmetric case because (as we explained previously) the effective resonance wavelength is larger for the antisymmetric excitation. The second resonance of the antisymmetric case occurs lower than 600 THz and varies from 402 THz (for $\Delta = 30^\circ$) to 554 THz (for $\Delta = 180^\circ$). For the symmetric case, the second resonance occurs higher than 700 THz according to Fig. 5(a) and varies as the angle Δ changes.

As a summary, by changing the polarization of the incident electric field from symmetric to antisymmetric, the resonant frequency of the V-shaped antenna shifted significantly. Moreover, the resonant frequency can be tuned by changing the angle Δ or the length L , i.e., we get two degrees of freedom. This is the geometrically tunable double-resonance property of the V-shaped plasmonic nanoantenna.

The other interesting observation in Figs. 5 and 6 is that by decreasing the angle Δ , the resonant frequency increases (blueshift) for the symmetric mode, and decreases (redshift) for the antisymmetric mode. For the special case in which Δ is small, because of the current directions for the arms connected at the junction, decreasing the angle Δ for the symmetric mode corresponds to having an equivalent nanorod with higher effective radius because the currents are in the same direction [see Fig. 1(b)]. This observation agrees with the result of the algebraic formula for the effective wavelength for a plasmonic nanorod given by Novotny [17], in which increasing the radius of the nanorod gives rise to a blueshift. For the antisymmetric mode with a small Δ , by considering the opposite directions for the current at the junction [Fig. 1(c)], the composite arm will have the smaller equivalent radius (because the joint currents cancel each other), which gives rise to a redshift. Also, because the currents tend to cancel each

other out (destructive effect), the peak of the scattered field for the small Δ in the antisymmetric mode decreases significantly [see Fig. 6(a)].

4. SCATTERING FROM PLASMONIC V-ANTENNA

Next, we compare the results with those obtained from the commercial software CST microwave studio (MWS), using both time and frequency domain solvers. The plasmonic V-antenna is made of silver whose permittivity is characterized by the Drude model that is described in Section 2. The arm length of the V-antenna is $L/2 = 75$ nm and the radius is $a = 7.5$ nm. The angle of the V-antenna is equal to $\Delta = 60^\circ$. The excitation is plane-wave with symmetric polarization [as demonstrated in Fig. 1(b)]. The frequency range for the incident plane wave is $100 \text{ THz} < f < 600 \text{ THz}$. The total (the sum of scattered and incident) field is measured by defining the electric field probes in CST MWS at $r = 0.2$ [μm] \hat{z} , which is $\lambda/2.5$ at higher frequency $f = 600$ THz, and thus in the near-field region for the frequency range mentioned above. The boundary condition is open for all six faces of the boundary box. The faces of the boundary box are $\lambda/4$ (at the lower frequency $f = 100$ THz) away from the origin (the junction of the V-antenna).

For the time domain solver in CST MWS, we have used ~ 28 million hexahedral mesh cells. In the mesh properties part of the CST MWS, we set “Line per wavelength” equal to 80 instead of the default value, which is 10. Moreover, in the CST local mesh properties, we define the local edge refinement factor equal to 10, instead of the default value 1, just to make sure that the thin arms of the plasmonic V-antenna are discretized very well in order to reach to a computational convergence for the energy convergence criterion equal to the -80 dB level. The CPU running time for the CST time domain solver is around 2 days on an Intel(R) Xeon(R) CPU having two 2.40 GHz processors. However it takes only 1 s/200 frequency samples for the MBF method on the same machine to compute the scattered field on the entire frequency band regardless of the location of the observation point.

For the frequency domain solver in CST MWS, we have used $\sim 800,000$ tetrahedral mesh cells. In the mesh properties part of the CST MWS, we set “steps per wavelength” equal to 6 instead of the default value, which is 4, just to make sure that the thin arms of the plasmonic V-antenna are discretized very well in order to reach to a computational convergence. The CPU running time for the CST frequency domain solver is around 1 day on the computer described above.

Figure 8 demonstrates the comparison between the scattered field obtained by MBFM, CST time domain, and CST frequency domain solvers. As we observe, the result of the CST frequency domain solver is pretty well matched to that of MBFM. For the CST time domain solver, the only difference is the magnitude of the peak of the resonance. This difference is due to the fact that the CST time domain solver needs a very fine mesh size for discretization of the arm cross-section of the plasmonic V-antenna. We already have the local mesh cell size equal to $a/24$ to discretize the cross-section of the plasmonic arms. Making the mesh size finer will drastically increase the CPU running time.

The radiation patterns for the V-shaped antenna in the x - y plane and in the plane including $\varphi = 120^\circ$ and $\varphi = 300^\circ$ are

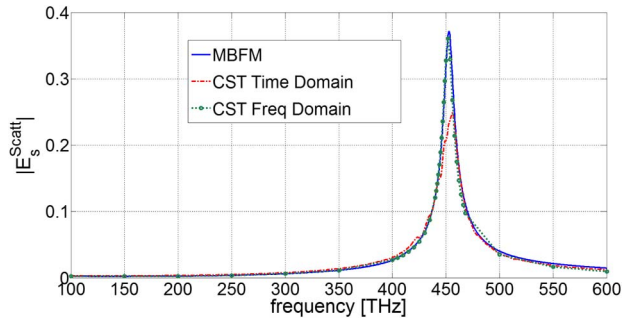


Fig. 8. Comparison of the MBF method and CST time and frequency domain solvers to compute the scattered field for the symmetric mode.

shown in Fig. 9 at $f = 450$ THz (resonance) for the symmetric excitation and for $\Delta = 60^\circ$. A good agreement between CST and MBF method is observed. In Fig. 9, we observe that the radiation pattern of the V-shaped antenna illuminated by the symmetric plane-wave excitation has a toroidal shape whose symmetric axis is along the bisector of the V-antenna, i.e., $\varphi = 30^\circ$. The physical reason is that, because of the symmetric excitation, the current distribution on each arm is the same (in magnitude and phase) and is close to the current distribution of a resonant dipole antenna. Thus, the x -arm and the v -arm

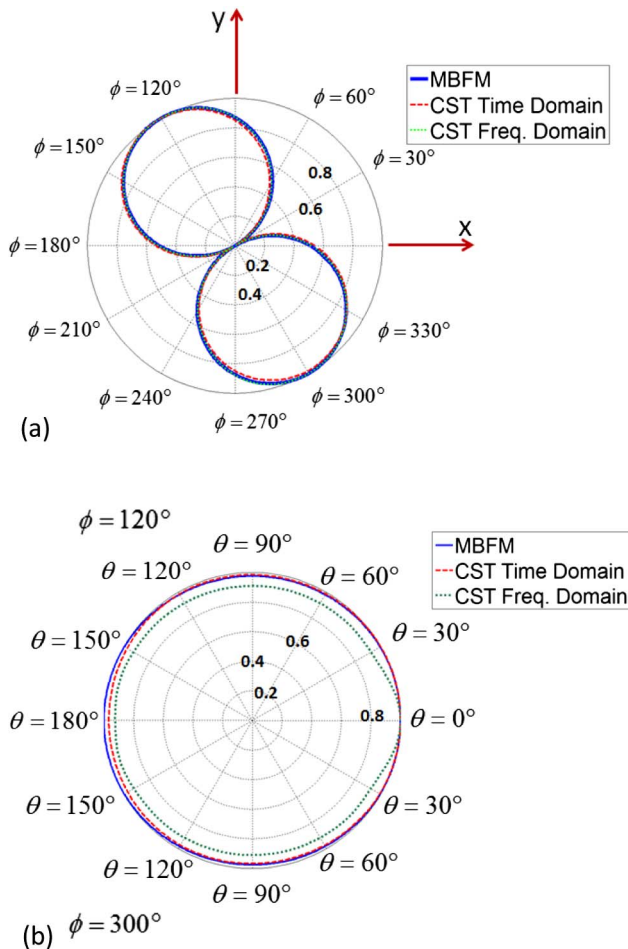


Fig. 9. Radiation pattern for the symmetric excitation and $\Delta = 60^\circ$ computed with MBF method (MBFM) compared to CST. (a) At $\theta = 90^\circ$ (xy plane). (b) At $\phi = 120^\circ$ (upper-half plane) and $\phi = 300^\circ$ (lower-half plane).

radiate toroidal-shaped patterns with the main lobes located at $\varphi_1 = \{90^\circ, 270^\circ\}$ and $\varphi_2 = \{150^\circ, 330^\circ\}$, respectively, in the x - y plane. Hence, the resultant superimposed pattern is a toroidal-shaped pattern with the main lobes placed at $\varphi_{\text{net}} = (\varphi_1 + \varphi_2)/2 = \{120^\circ, 300^\circ\}$, according to Fig. 9(a) in the x - y plane. The radiation pattern is omnidirectional [see Fig. 9(b)] at the plane φ_{net} comprised of $\varphi = 120^\circ$ and $\varphi = 300^\circ$.

5. CONCLUSIONS

In this work, we have introduced a computationally efficient, strong, and fast technique to analyze the scattering of an optical planewave from a plasmonic V-shaped nanoantenna. Our technique is based on MBFM, which leads to a small-sized and well-conditioned matrix equation constructed using closed-form formula for the electric field radiated by piecewise sinusoidal MBFs. The technique explained in our work is 4 to 10 orders of magnitude faster than the time-domain and frequency-domain solvers in CST MWS. Our computational scheme can be used as a powerful engine for efficient analysis and design optimization of large arrays of plasmonic configurations comprised of junctions of monopoles.

ACKNOWLEDGMENTS

This work was supported by the Defense Advanced Research Projects Agency (DARPA)/Microsystems Technology Office (MTO) Young Faculty Award program under Award No. N66001-11-1-4145, the National Science Foundation under grants ECS-1310400, ECS-1310257, and IIP-1417284, and the Hellenic Ministry of Education project Thales RF-Eigen-Sdr. The authors thank Dr. M. Al-Tarifi for his help with CST simulations.

REFERENCES

1. H. A. Atwater and A. Polman, "Plasmonics for improved photovoltaic devices," *Nat. Mater.* **9**, 205–213 (2010).
2. L. Novotny and B. Hecht, *Principles of Nano-Optics* (Cambridge University, 2006).
3. T. H. Taminiau, R. J. Moerland, F. B. Segerink, L. Kuipers, and N. F. van Hulst, " $\lambda/4$ resonance of an optical monopole antenna probed by single molecule fluorescence," *Nano Lett.* **7**, 28–33 (2007).
4. A. Alù and N. Engheta, "Input impedance, nanocircuit loading, and radiation tuning of optical nanoantennas," *Phys. Rev. Lett.* **101**, 043901 (2008).
5. B. Lounis and M. Orrit, "Single-photon sources," *Rep. Prog. Phys.* **68**, 1129–1179 (2005).
6. P. Biagioni, J. S. Huang, L. Duò, M. Finazzi, and B. Hecht, "Cross resonant optical antenna," *Phys. Rev. Lett.* **102**, 256801 (2009).
7. P. Biagioni, M. Savoini, J. Huang, L. Duò, M. Finazzi, and B. Hecht, "Near-field polarization shaping by a near-resonant plasmonic cross antenna," *Phys. Rev. B* **80**, 153409 (2009).
8. E. S. Ünlü, R. U. Tok, and K. Şendur, "Broadband plasmonic nanoantenna with an adjustable spectral response," *Opt. Express* **19**, 1000–1006 (2011).
9. N. Yu, P. Genevet, M. A. Kats, F. Aieta, J. Tetienne, F. Capasso, and Z. Gaburro, "Light propagation with phase discontinuities: generalized laws of reflection and refraction," *Science* **334**, 333–337 (2011).
10. Q. Xu, J. Bao, R. M. Rioux, R. Perez-Castillejos, F. Capasso, and G. M. Whitesides, "Fabrication of large-area patterned nanostructures for optical applications by nanoskiving," *Nano Lett.* **7**, 2800–2805 (2007).
11. M. Sukharev, J. Sung, K. G. Spears, and T. Seideman, "Optical properties of metal nanoparticles with no center of inversion symmetry: observation of volume plasmons," *Phys. Rev. B* **76**, 184302 (2007).

12. A. Taflove and S. C. Hagness, *Computational Electromagnetic: The Finite-Difference Time-Domain Method* (Artech, 2005).
13. A. Rashidi, H. Mosallaei, and R. Mittra, "Scattering analysis of plasmonic nanorod antennas: a novel numerically efficient computational scheme utilizing macro basis functions," *J. Appl. Phys.* **109**, 123109 (2011).
14. A. Rashidi, H. Mosallaei, and R. Mittra, "Macro basis functions for accurate and fast solution of scattering from elements comprising of junctions of wires and strips," in *2011 IEEE International Symposium on Antennas and Propagation (APSURSI)*, (IEEE, 2011), pp. 646–649.
15. A. Rashidi and H. Mosallaei, "Scattering performance of plasmonic nanorod antennas in randomly tilted disordered and Fibonacci configurations," *Appl. Phys. Lett.* **101**, 061105 (2012).
16. R. F. Harrington, *Time-Harmonic Electromagnetic Fields* (IEEE, 2001).
17. L. Novotny, "Effective wavelength scaling for optical antennas," *Phys. Rev. Lett.* **98**, 266802 (2007).